# A THEORETICAL ANALYSIS OF LOCAL THERMAL EQUILIBRIUM IN FIBROUS MATERIALS

by

***Mingwei TIAN*** [a, b*], ***Ning PAN*** [c, d], ***Lijun QU*** [a, b], ***Xiaoqing GUO*** [a, b], ***and Guangting HAN*** [b]

[a] College of Textile and Clothing, Qingdao University, Qingdao, China
[b] Collaborative Innovation Center for Marine Biomass Fibers, Materials and Textiles of Shandong Province, Qingdao University, Qingdao, China
[c] Institute of Physics of Porous Soft Matters, Donghua University, Shanghai, China
[d] Biological and Agricultural Engineering Department,University of California, Davis, Cal., USA

Original scientific paper
DOI: 10.2298/TSCI120607018T

*The internal heat exchange between each phase and the local thermal equilibrium scenarios in multi-phase fibrous materials are considered in this paper. Based on the two-phase heat transfer model, a criterion is proposed to evaluate the local thermal equilibrium condition, using derived characteristic parameters. Furthermore, the local thermal equilibrium situations in isothermal/adiabatic boundary cases with two different heat sources (constant heat flux and constant temperature) are assessed as special transient cases to test the proposed criterion system, and the influence of such different cases on their local thermal equilibrium status are elucidated. In addition, it is demonstrated that even the convective boundary problems can be generally estimated using this approach. Finally, effects on local thermal equilibrium of the material properties (thermal conductivity, volumetric heat capacity of each phase, sample porosity, and pore hydraulic radius) are investigated, illustrated, and discussed in our study.*

Key words: *porous fibrous media, local thermal equilibrium, boundary conditions, material property and structure*

## Introduction

It is universally acknowledged that Fourier's law can be treated as the classical fundamental theory of heat conduction for single-phase material in thermal equilibrium, and it may however not be automatically applied to multi-phase heat transfer problems. Multi-phase materials, such as foam metal, fibrous material, catalytic reactors and other mixtures, consist of different phase components whose properties are in general discrepant significantly. In other words, the heat transfer ability of each phase and hence its corresponding thermal status differ from each other, rendering the system more prone to be in thermal non-equilibrium, especially at the local levels. Therefore the original Fourier's law is in general not applicable to such issue.

Over the past decades, many studies have been done to remedy this problem. Cattaneo [1] and Vernotte [2] established the thermal wave equation to define the non-Fourier's problems

* Corresponding author; e-mail: tmw0303@126.com

and proposed the relaxation time to determine the finite velocity of the heat flow. Tzou [3] modified the thermal wave equation and proposed the phase-lag concept to describe the lagging behavior of heat conduction from macro- to micro-scales. Amiri and Vafai [4] then applied the phase-lag theory to establish the governing equations for two-phase porous media and analyzed the boundary and inertia effects. Nield *et al.* [5] presented an analytic solution for the forced convection in a saturated porous medium limited by a parallel-plane channel. Besides, Kuznetsov *et al*. [6] established that the temperature difference between the fluid and solid phases forms a thermal wave localized in space and derived an analytical solution for this wave. Through extensive research, it has become clear now that the key issue in dealing with heat transfer in multi-phase materials is to determine if there is a local thermal equilibrium (LTE) established among the different phases, for at such a LTE condition, the local temperatures of the adjacent phases are nearly equal to each other and the lag time becomes negligible so that the Fourier's law is valid again for the entire system. Otherwise, the material is considered at Local thermal non-equilibrium (LTNE) such that the local discrepancy in thermal state between different phases cannot be neglected.

As such, researchers have developed several criteria to assess the LTE situation using specific multiphase models. For instance, Minkowycz *et al*. [7] derived a dimensionless parameter, *Sp*, to estimate the LTE conditions. Moreover, Lee andVafai [8] classified the heat transfer characteristics into three regimes, each dominated by one of the three distinctive heat transfer mechanisms, so as to deal with them separately. Yang *et al*. [9] investigated the gradient bifurcation between the fluid phase and solid matrix to determine the LTE behavior. Vadasz [10] calculated the phase temperatures in both steady and transient conditions using analytical methods and demonstrated that a system will always be in LTE under the steady-state, and turns to LTNE during the transient process. Zhao *et al*. [11], Shi and Yu [12], Li and He [13], Li [14], He *et al*. [5] , Fan *et al.* [16], and Yang *et al*. [17] introduced some alternative fractal approaches to such problems. In addition, some works tackled other related yet more specific issues like the forced convective incompressible flow through porous beds [18], local thermal non-equilibrium with internal heat generation [19], porous medium in heat exchanger [20, 21], and the heat exchange between human tissues and blood flow [22, 23]. Most of these investigations focused on analyzing and determining what thermal state a specific porous material is in (LTE or LTNE). However given the significance of LTE related issues in heat transfer processes, it is our opinion that more detailed investigations on the problems are desirable for better understanding of the phenomenon.

The objective of this work is to first develop a more thorough understanding of the internal heat transfer in fibrous materials, the temperature distributions in both fiber and air phases and the relations between them by employing an analytical method [7], then to propose a new and hopefully more effective criterion to assess the system LTE status. After the assessment system is developed, actual problems with two bounds (isothermal and adiabatic) heated by two different heat sources (constant heat flux and constant temperature) are examined, as testing cases for our approach to study their influences. Also it is demonstrated that the LTE conditions of these two bounds can be used to deal with convection boundary cases. Finally some numerical studies are conducted, dealing with the effects of the thermal properties, material structure of porous materials on the LTE behavior.

## Heat conduction by two-phase fibrous materials

Fibrous materials as typical two-phase porous media are composed of fibers and air, if neglecting the moisture contained [24]. A scaning electron microscope example of such a po-

rous structure is shown in fig. 1 [25] where the fibers are interlaced in the system. When the sample is exposed to a thermal agitation, the internal heat transfer and energy exchange between the two phases occur.

When the porous structure is assumed structurally isotropic and the thermophysical properties are independent of temperature, the governing equation for each phase can be obtained from the energy conservation based on the local volume average theory [4, 26]:

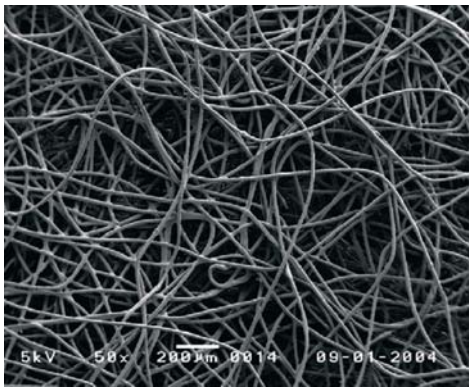


**Figure 1. A SEM picture of non-woven fibrous material**

$$\varepsilon\rho C_{\mathrm{a}}\frac{\partial T_{\mathrm{a}}(x,t)}{\partial t}+\rho C_{\mathrm{a}}U\nabla T_{\mathrm{a}}= =-\nabla q_{\mathrm{a}}(x,t)+h_{\mathrm{e}}a_{\mathrm{af}}(T_{\mathrm{f}}-T_{\mathrm{a}}) \quad (1a)$$

$$(1-\varepsilon)\rho C_{\mathrm{f}}\frac{\partial T_{\mathrm{f}}(x,t)}{\partial t}=-\nabla q_{\mathrm{f}}(x,t)-h_{\mathrm{e}}a_{\mathrm{af}}(T_{\mathrm{f}}-T_{\mathrm{a}}) \quad (1b)$$

where $T_{\mathrm{a}}(x, t)$ and $q_{\mathrm{a}}(x, t)$ are the volume averaged temperature and heat flux for the air phase over a representative localized volume, while $T_{\mathrm{f}}(x, t)$ and $q_{\mathrm{f}}(x, t)$ are for the fiber phase; $\rho C_{\mathrm{a}}$ and $\rho C_{\mathrm{f}}$ are the volumetric heat capacity of air and fiber, respectively and $\varepsilon$ is the porosity of the system; other parameters listed in the equation are: $h_{\mathrm{e}}$ is the interstitial heat transfer coefficient between the two phases, $\vec{\mathrm{U}}$ – the fluid velocity vector and $a_{\mathrm{af}}$ the specific surface area of the material pores.

Summing eq. (1a) and (1b) up and considering the influence of the volumetric heat source $S(x, t)$ results in:

$$\varepsilon\rho C_{\mathrm{a}}\frac{\partial T_{\mathrm{a}}(x,t)}{\partial t}+\rho C_{\mathrm{a}}\vec{\mathrm{U}}\nabla T_{\mathrm{a}}+(1-\varepsilon)\varepsilon\rho C_{\mathrm{f}}\frac{\partial T_{\mathrm{f}}(x,t)}{\partial t}=-\nabla q(x,t)+S(x,t) \quad (1c)$$

where $q(x, t) = q_{\mathrm{a}}(x, t) + q_{\mathrm{f}}(x, t)$ is the total heat transfer through the representative localized volume.

Assuming the heat released from the fibers is totally absorbed by its surrounding air phase at a local level, the energy conservation $Q = Cm\Delta T$ yields the relation:

$$\rho C_{\mathrm{a}}\Delta V_{\mathrm{p}}\frac{\partial T_{\mathrm{a}}(x,t)}{\partial t}=h_{\mathrm{e}}\Delta A_{\mathrm{p}}[T_{\mathrm{f}}(x,t)-T_{\mathrm{a}}(x,t)] \quad (2a)$$

or converting into:

$$T_{\mathrm{f}}(x,t)-T_{\mathrm{a}}(x,t)=\frac{\Delta V_{\mathrm{p}}\rho C_{\mathrm{a}}}{h_{\mathrm{e}}\Delta A_{\mathrm{p}}}\frac{\partial T_{\mathrm{a}}(x,t)}{\partial t}=\frac{r_{\mathrm{h}}\rho C_{\mathrm{a}}}{h_{\mathrm{e}}}\frac{\partial T_{\mathrm{a}}(x,t)}{\partial t} \quad (2b)$$

where $\Delta V_{\mathrm{p}}$ and $\Delta A_{\mathrm{p}}$ are the volume and the surface area of a mean pore and their ratio $\Delta V_{\mathrm{p}}/\Delta A_{\mathrm{p}}$ is termed as the pore hydraulic radius $r_{\mathrm{h}}$. If the local heat exchange between the two adjacent phases is not sufficient due to their property disparities, the local temperature discrepancy appears in the representative localized volume, and the system is thus considered at local thermal non-equilibrium (LTNE) condition.

At the LTNE conditions, the Fourier equation $q(x, t) = -k_{\mathrm{e}}\nabla T(x, t)$ does not hold any more, but some works [3, 7] have established the modified equation of Fourier equation under the LTNE conditions as:

$$q(x,t)+\tau_q\frac{\partial q(x,t)}{\partial t}=-k_e\left\{\nabla T_a(x,t)+\tau_t\frac{\partial}{\partial t}[\nabla T_a(x,t)\right\} \tag{3}$$

where $k_e = \varepsilon k_a + (1-\varepsilon)k_f$ is the equivalent thermal conductivity for the multi-phase material where $k_a$ and $k_f$ correspond to the air and fiber phases. In addition, two lag times ($\tau_q$ and $t_t$) can be interpreted as $\tau_q$ – the relaxation time resulted from the fast-transient effect due to thermal inertia of heat flux and is named the heat flux phase-lag and can be expressed as $\tau_q \approx \rho C_f R_c \Delta V_f/\Delta A_f$ [27], whereas $\tau_t$ – the parameter describing the time delay in temperature gradient across the differential phase and $\tau_t \approx r_h \rho C_a/h_e$ as shown in eq. (2b).

In the present work, several typical boundary conditions (B.C.) in porous material applications are discussed, shown in fig. 2 corresponding to the mathematical forms in tab. 1. Both B.C.1 and B.C.2 are the representative cases under the constant heat sources, while B.C.3 and B.C.4 are heated by the constant temperature sources in fig. 2. Their initial conditions are all set as the same temperature $T_0$. The processes of solving the above governing equations under the B.C.1-4, respectively, are provided in the Appendix by employing an analytical method [7], where the dimensionless temperature distributions for each phase have been obtained.

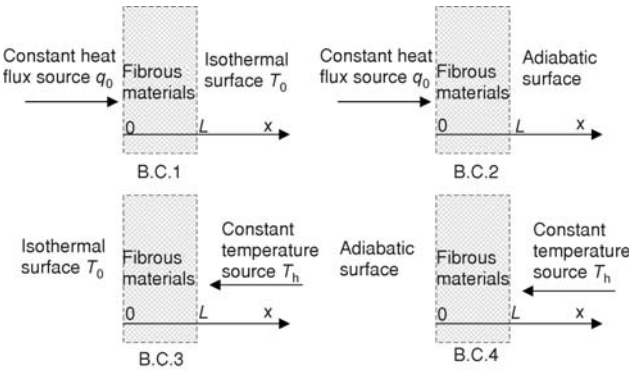


**Figure 2. Schematic digammas of the boundary conditions**

**Table 1. four different boundary conditions**

| | B.C.1 | B.C.2 | B.C.3 | B.C.4 |
|---|---|---|---|---|
| $x = 0$ | $k_a\frac{\partial T_a}{\partial x}=k_f\frac{\partial T_f}{\partial x}=-q_0$ | $k_a\frac{\partial T_a}{\partial x}=k_f\frac{\partial T_f}{\partial x}=-q_0$ | $T_a=T_f=T_0$ | $\frac{\partial T_a}{\partial x}=\frac{\partial T_f}{\partial x}=0$ |
| $x = L$ | $T_a=T_f=T_0$ | $\frac{\partial T_a}{\partial x}=\frac{\partial T_f}{\partial x}=0$ | $T_a=T_f=T_h$ | $T_a=T_f=T_h$ |
| Initial condition $t = 0$ | $T_a=T_f=T_0$ | $T_a=T_f=T_0$ | $T_a=T_f=T_0$ | $T_a=T_f=T_0$ |

## A criterion of local thermal equilibrium in fibrous materials

Once obtaining the temperature distribution for each phase, we can facilely obtain the local discrepancy between the contacting phases in the localized representative volume. This discrepancy solely determines the internal LTE behavior, *i. e.*, the bigger the discrepancy, the deeper the system into the LTNE condition. The local discrepancy $\Delta\theta$ between the dimensionless temperature distributions of the two phases can be expressed as:

$$\Delta\theta=\theta_a-\theta_f \tag{4}$$

where $\theta_a$ and $\theta_f$ are the dimensionless temperatures for the air and fiber phases derived from Appendix. Therefore, the porous material can be treated as in the LTE conditions once this discrepancy $\Delta\theta < \Delta\theta_{cv}$, *i. e.*, becoming smaller than a critical value $\Delta\theta_{cv}$ (= 0.0001 in our study).

In our discussions below, the isothermal case B.C.1 is chosen as an example to study the local discrepancy $\Delta\theta$ between the thermal states of the two phases. The sample thickness $L$ and heat source flux $q_0$ are set at 0.01m and 100 W/m$^2$, the fiber volumetric heat capacity $\rho C_f$ is $5\cdot10^5$ J/m$^3$K and the properties of the air phase are given as $k_a$ = 0.025 W/mK and $\rho C_a$ = $=1.21\cdot10^3$ J/m$^3$K from ref. [28, 29]. Other parameters at the default values are in tab. 2.

**Table 2. The properties used in computation**

| Physical property | Fiber phase $k_f$ [Wm$^{-1}$K$^{-1}$] | Pore hydraulic radius $r_h$ [m] | Fiber phaser $C_f$ [Jm$^{-3}$K$^{-1}$] | Porosity $\varepsilon$ |
|---|---|---|---|---|
| Default value | 0.10 | $5.0\cdot10^{-4}$ | $1.0\cdot10^5$ | 0.80 |
| Range | 0.05~2.50 | $5.0\cdot10^{-5}$~$1.0\cdot10^{-3}$ | $2.0\cdot10^3$~$1.0\cdot10^6$ | 0.05~0.95 |

The local discrepancy curves $\Delta\theta$ in fig. 3, illustrate the phase-lag in temperature of the sample against time, at different locations $x$. The curves exhibit a similar trend, increasing from the origin, reaching the peaks and then falling off to zero. We can then define two time markers ($t_{min}$ and $t_{max}$) between the curves using the critical value $\Delta\theta_{cv}$, so as to symbolize the entry and exit moments of the LTNE condition. The net length between these two moments ($\Delta t$ = $= t_{max} - t_{min}$) represents the duration stayed in the LTNE condition. Thus the two time points ($t_{min}$ and $t_{max}$) and the duration ($\Delta t$) can be used logically as the parameters to assess the LTE condition of a porous system. Here, intrinsically, $\Delta t$, the duration of LTNE, characterizes the effective transit period of the entire heat transfer process, and the rest time can be treated as in the LTE state, including the steady-state period and the residual transient period, with negligible marginal local discrepancy $\Delta\theta < \Delta\theta_{cv}$.

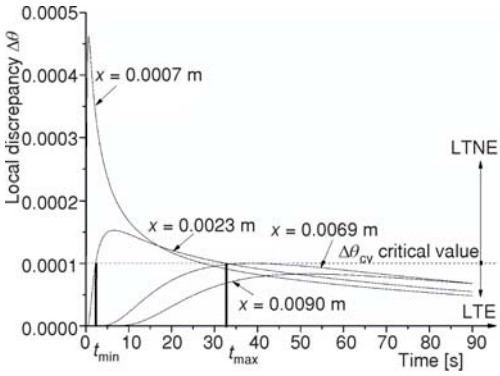


**Figure 3. Local discrepancy of samples at $x$ = 0.0007 m, 0.0023 m, 0.0069 m, and 0.0090 m, respectively, in B.C.1 model, the dotted horizontal line is the critical value $\Delta\theta_{cv}$ = 0.0001**

These two time markers are clearly functions of many related variables:

$$t_{min} = f_1\left(k_f, \rho C_f, \varepsilon, r_h, \frac{\partial T_a}{\partial t}, T_{st}^*\right), \quad t_{max} = f_2\left(k_f, \rho C_f, \varepsilon, r_h, \frac{\partial T_a}{\partial t}, T_{st}^*\right) \tag{5}$$

where $T_{st}^*$ is the steady-state temperature in each boundary case made available in Appendix. That is, these two parameters are not only related to the intrinsic properties of the material system (fiber phase thermal conductivity $k_f$, volumetric heat capacity $\rho C_f$, porosity $\varepsilon$, and pore hydraulic radius $r_h$) but also to the temperature slope $\partial T_a/\partial$t and $T_{st}^*$.

Returning to fig. 3 where four curves of the same sample are shown, corresponding to different locations in the sample $x$ = 0.0007 m, 0.0023 m, 0.0069 m, and 0.0090 m, it is clear first that in the same sample but at the locations sufficiently further away from the heat source ($x \geq 0.0069$ m), the system is always at the LTE condition throughout the time based on the criterion $\Delta\theta < \Delta\theta_{cv}$ so that the local temperature discrepancy between the air and solid fiber can be neglected. It is only at the locations within $x < 0.0069$ m that LTNE becomes a concern – the

closer the location, *i. e.*, a smaller $x$, the earlier for the location to enter LTNE state. In other words, during a thermal transfer process in a porous material with constant heat source, only the parts close enough to the heat source experience the local thermal non-equilibrium state.

### Thermal responses at different boundary conditions

In this section, the equilibrium status of both boundary (isothermal/adiabatic), and heat source conditions (constant heat flux/temperature) listed in fig. 2 are discussed so as to exhibit the differences between them. We then found out from our calculations that not only such differences are huge, but they depend on the fiber thermophysical properties ($k_f$ and $\rho C_f$) and sample structure properties ($\varepsilon$) as well. Nonetheless a complete graphic illustration of such influence of different boundary conditions, at all possible ranges of the properties, is too complex to present in one drawing, we only provided a few special cases with some fixed properties in figs. 4 and 5, just to show the differences. Whereas simpler cases hence with more comprehensive illustrations are shown in figs. 7 in 3-D plotting where one can get the sense of the difficulties involved.

The distributions of $t_{min}$, $t_{max}$, and $\Delta t$ for B.C.1~4 are illustrated in figs. 4 and 5 using the boundary conditions listed in tab. 1 and the data in tab. 2. Conditions B.C.1 and 2 are both heated by the same constant heat flux source ($q_0 = 100$ W/m$^2$), while B.C.3 and 4 by the constant temperature source ($T_h = 10$ °C). The initial temperature of these four cases are all set as $T_0 = 0$ °C.

First, in both B.C.1 and 2 cases in fig. 4(a) and (b), $t_{min}$, $t_{max}$ and $\Delta t$ simultaneously increase against the distance $x$, meaning that at locations further away from the heat source ($x = 0$), the entry ($t_{min}$) and exit ($t_{max}$) moments to LTNE stage are both delayed, and the duration ($\Delta t$) in LTNE is extended.

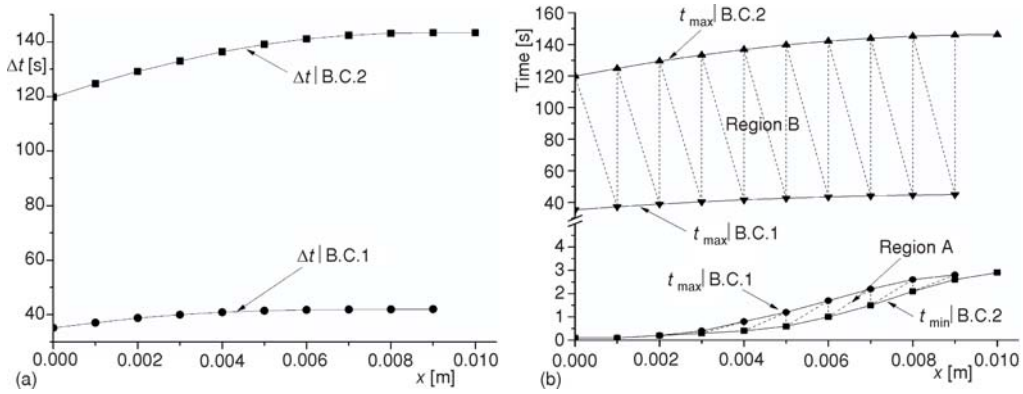


**Figure 4. The relationship between the parameters and the position $x$ for conditions B.C.1 and B.C.2, (a) $\Delta t$ -$x$, (b) $t_{min}$, $t_{max}$ -$x$**

From fig. 4(a) and (b), we can also conclude that the isothermal case B.C.1 possesses a greater tmin but smaller tmax than the adiabatic case B.C.2, resulting in a much shorter duration $\Delta t$. The differences are attributed to the nature of the boundary settings: at the isothermal condition B.C.1 with a higher heat leaking from the other end, the sample is only able to retain a lower temperature level, unlike the adiabatic B.C.2 surface where no heat leaks out at all.

Whereas for B.C.3 and 4 boundary conditions with constant heat temperature source ($T_h = 10$ °C), assuming the source located at $x = 0.01$ m, at that point both the fiber and air phases

possess the same temperature ($T_f = T_a = T_h$) and thus always at LTE condition. Once moving away from the heat source however, seen from fig. 5(a), the samples enter the LTNE state. Overall, the isothermal case B.C.3 stays in the LTNE state shorter, indicated by a smaller $\Delta t$ value in fig. 5(a), but enters and leaves the LTNE state earlier, by smaller $t_{min}$ and $t_{max}$ values in fig. 5(b), than the adiabatic B.C.4 case. The results can be explained in thermal physics terms. Since the isothermal B.C.3 surface leaks more heat than the B.C.4 case, it thus requires greater heat supply from the heat source to maintain its constant temperature ($T_h$) at the other end. Such heat has to be transferred through the same material over the same distance from the heat source, the heat transfer rate in B.C. 3 has to be higher so that both the entry time ($t_{min}$) and exit time ($t_{max}$) of LTNE in B.C.3 are earlier than those in B.C.4, leading to overall a smaller duration $\Delta t$ than in B.C.4.

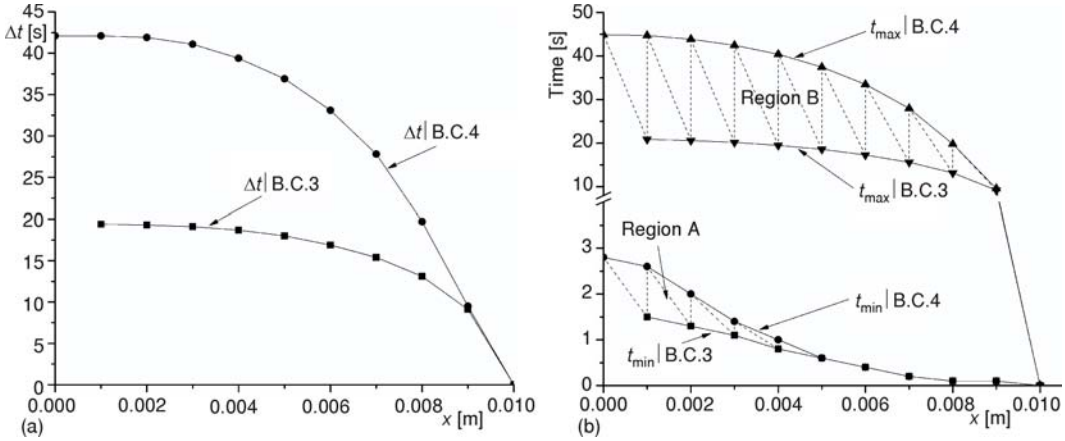


**Figure 5. The relationship between the parameters and the position *x* for conditions B.C.3 and B.C.4, (a) $\Delta t$ -x, (b) $t_{min}$, $t_{max}$- *x***

Furthermore, as the thermal responses of samples under convection boundaries are considered to be all within the isothermal and adiabatic boundary conditions [30], the LTE state for such convection cases can also be estimated here based on the two extreme cases. That is, the isothermal and adiabatic boundaries can be viewed as the special cases of all the convection boundary cases, with the maximum and minimum convection coefficients, respectively. For all convection situations $t_{min}$, $t_{max}$ and $\Delta t$ are located between these two bounds as indicated in figs. 4(b) and 5(b), where region A are the corresponding LTNE entry moments ($t_{min}$), and Region B are the estimated exit moments ($t_{max}$) for all the convection cases.

The boundary conditions of actual fibrous materials are more complex than the cases dealt with here, *e. g*., with different initial conditions of internal phases, samples with three or more phases, and multi-dimension heat transfer, *etc*., and their corresponding LTE status will be more erratic. But the approach proposed in this paper can still be useful as an approximate and simply way to study the LTE behaviors of these complex cases.

## Effects of several key parameters on the sample LTE behavior

In this section, the influences of the fiber thermophysical properties ($k_f$ and $\rho C_f$) and sample porosity $\varepsilon$ and pore hydraulic radius $r_h$ on the system parameters ($t_{min}$, $t_{max}$, and $\Delta t$) are discussed, again using B.C.1 as the example. The ranges of the related parameters in our compu-

tation are from tab. 2: when dealing with one parameter, others will always take the default values, and the heat source flux $q_0$ is fixed at 100 W/m$^2$.

*Influence of the fiber thermal conductivity*

The fiber thermal conductivity $k_f$ within the range in tab. 2 is used to calculate the results drawn in fig. 6. The value of $\Delta t$ decreases with the increased $k_f$ in fig. 6(a), and the other two parameters ($t_{min}$ and $t_{max}$) in fig. 6(b) exhibit the similar trend. The influence of sample location $x$ as seen from the curves is also quite simple.

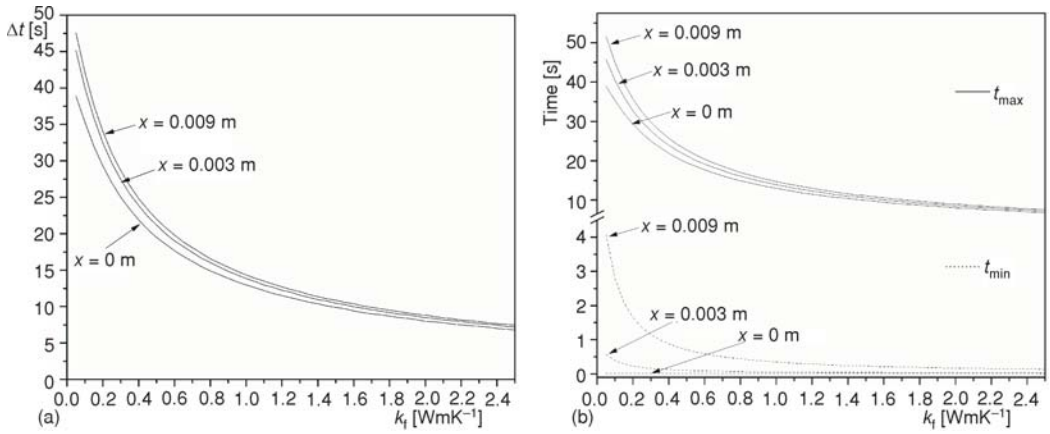


**Figure 6. Effect of the fiber thermal conductivity $k_f$ on the parameters, (a) for $\Delta t$ and (b) for $t_{min}$ and $t_{max}$**

Thermal conductivity by definition is the specific amount of the heat that passes the cross-section of an object. Since in B.C.1 case with constant heat supply for the porous sample, the sample with bigger $k_f$ can thus transfer heat more quickly to the entire sample, so its temperature rises earlier and the slope becomes steeper, leading to a smaller entry time ($t_{min}$). However, as this high transfer ability will also leak more heat to the external environment more quickly and thus more difficult to maintain the temperature, it leads to an end moment ($t_{max}$) earlier than the sample with smaller $k_f$. In other words, the fiber thermal conductivity is an important factor in affecting the LTE conditions, the higher the $k_f$ value, the earlier LTNE appears, but overall the shorter LTNE period for the sample. Also, remembering what demonstrated in the section *A criterion of local thermal equilibrium in fibrous materials*, the curves of $t_{min}$ and $t_{max}$ here can be used as the limitting cases for the convection problems.

*Influence of fiber volumetric heat capacity*

The influence of fiber volumetric heat capacity $\rho C_f$ is given in fig. 7, in 3-D due to the complicities caused by having to include the sample location $x$ as well. It is shown in fig. 7(a) that, location $x$ exerts a significant impact on the LTNE duration $\Delta t$: when the location in the sample is sufficiently further away from the heat source ($x \gg 0$), the sample will not experience the LTNE state at all as long as the sample volumetric heat capacity $\rho C_f$ is not too small. However, at other location $x$, the influence of $\rho C_f$ on $\Delta t$ shows a parabola pattern: $\Delta t$ increases from zero to a maximum and then drops back to near zero as $\rho C_f$ decreases from its maximum to close to 0.

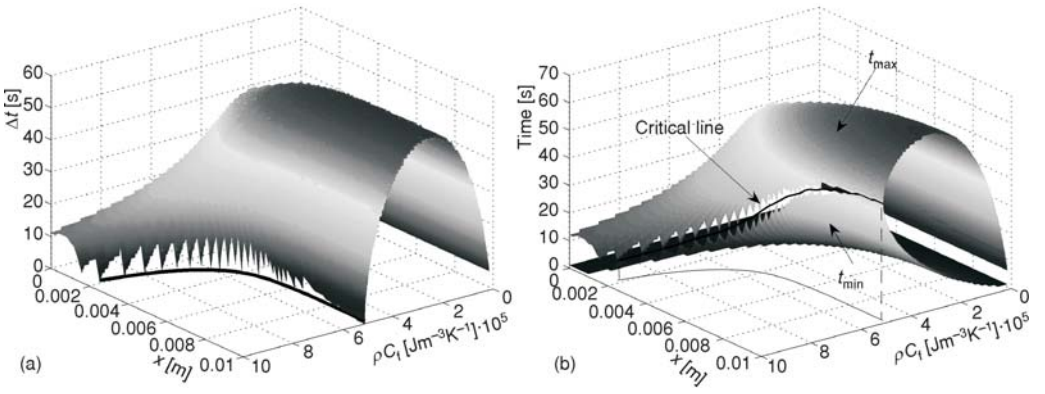


**Figure 7. Effect of the fiber volumetric heat capacity $\rho C_f$ on the parameters, (a) for $\Delta t$ and (b) for $t_{min}$ and $t_{max}$**

Correspondingly, the influences of both position $x$ and $\rho C_f$ on the entry time $t_{min}$ in fig. 7(b) are very similar to fig. 7(a) on $\Delta t$. Whereas the profiles on the exit time $t_{max}$ is such that combined with those for $t_{min}$, an unsymmetrical tubular 3-D hyper-plane is formed where two parabola curved planes for $t_{min}$ and $t_{max}$ connected at a critical line, meaning the entry and exit moments converge ($t_{min} = t_{max}$) and the LTNE duration degenerates to zero. Note the 3-D connecting critical line is projected into the 2-D line in fig. 7(b).

### *The influence of sample porosity*

Porosity $\varepsilon$, a key parameter of material structure, is specified in this section and its relationship with the characteristic parameters is plotted in fig. 8. Porosity $\varepsilon$ is defined as the fraction of the volume of voids over the total volume. In a porous material, increasing $\varepsilon$ or the air volume fraction shifts the thermal response of the material towards more dominance by the air phase which possesses significantly smaller thermal conductivity and volumetric heat capacity than the fiber phase. Hence, heated by the constant heat flux in B.C.1, the samples with greater porosity holding more air will experience a quicker temperature rise and reach the steady-state condition earlier, *i. e.*, the corresponding times $t_{min}$ and $t_{max}$ both arrive earlier and the duration $\Delta t$ tends to be smaller, as illustrated in figs. 8(a) and (b).

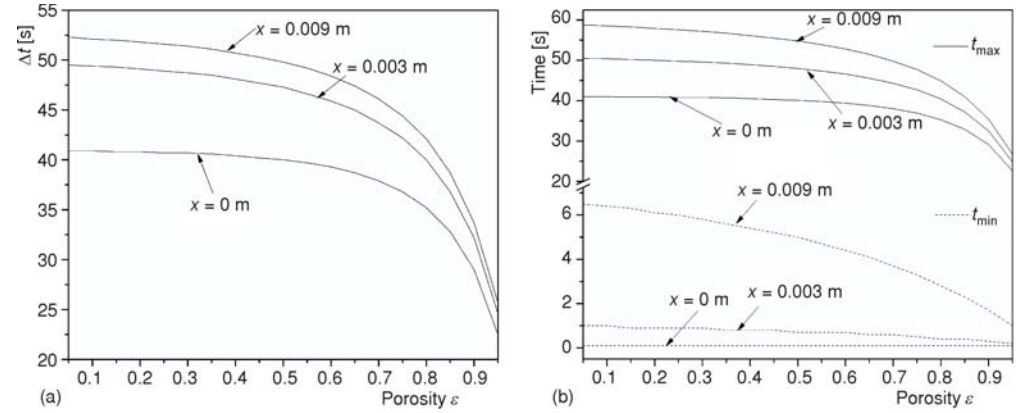


**Figure 8. Effect of porosity $\varepsilon$ on the parameters, (a) for $\Delta t$ and (b) for $t_{min}$ and $t_{max}$**

*The influence of sample pore hydraulic radius*

Pore hydraulic radius $r_h$ plays an important role in $\Delta t$, and also impacts on $t_{min}$ and $t_{max}$ from fig. 9(a) and (b). $\Delta t$ and $t_{max}$ are both proportionate to the $r_h$ while $t_{min}$ with the inversely-proportional relationship. A bigger $r_h = \Delta V_p/\Delta A_p$ means that the specific contacting surfaces between local air and fiber phase are smaller, so the heat exchange may be more inefficient, according to eq. (2), then the time of local discrepancy increasing to the critical value $\Delta\theta_{cv}$ becomes earlier and decreasing to $\Delta\theta_{cv}$ becomes later, so $t_{min}$ and $t_{max}$, respectively, become smaller and bigger with a larger $r_h$. We also can find that $t_{min}$ and $t_{max}$ overlap at the critical line, which means that the LTNE can be avoided once the $r_h$ is small enough.

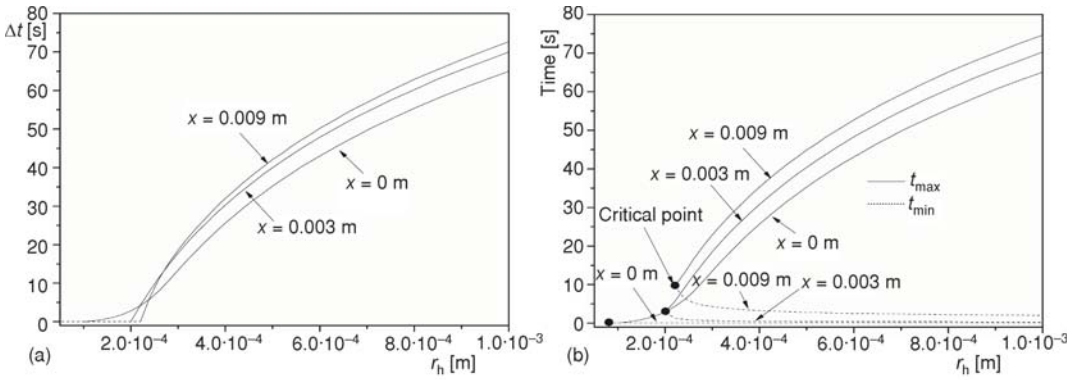


**Figure 9. The effect of $r_h$ on the parameters, (a) for $\Delta t$ and (b) for $t_{min}$ and $t_{max}$**

## Conclusions

By using the heat transfer theory for fibrous porous materials, we calculated the local discrepancy of adjacent two phases (air/fiber) to establish a criterion; this criterion can be used to determine the LTE condition for porous media, using three characteristic parameters, the entry and exit moments of LTNE $t_{min}$ and $t_{max}$, and the duration in LTNE stage $\Delta t$.

Four common boundary conditions were employed to study the influence of boundary conditions. Heated by the same constant heat flux source, the isothermal case possessed a bigger $t_{min}$ and smaller $t_{max}$ than the adiabatic case, so the former enters LTNE later and stays there for a short period $\Delta t$ than the latter. Under the constant temperature source, the isothermal model is in and out of the LTNE stage earlier than the adiabatic one, resulting an overall shorter duration $\Delta t$.

The isothermal and adiabatic boundaries can be viewed as the special cases of all the convection boundary cases, with the maximum and minimum convection coefficients, respectively. For all convection situations $t_{min}$, $t_{max}$, and $\Delta t$ are located between these two bounds. In other words, the LTNE behavior of convection boundaries could be generally estimated from the region rounded by the two bounds (isothermal/adiabatic).

As to the influences of the fiber thermophysical properties ($k_f$ and $\rho C_f$) and material porosity $\varepsilon$ and pore hydraulic radius $r_h$ on thermal behaviors of porous media, increasing any one of $k_f$, $\rho C_f$, and $\varepsilon$ will reduce and even eliminate the region of LTNE status in the case (isothermal with constant heat flux) conditions. Our theoretical approach can be extended to assess the LTE conditions of some other complex, dynamic, and multiscale cases.

## Acknowledgment

Financial support of this work was provided by Natural Science Foundation of China via grant no. 51306095 and 51273097 and Taishan scholars construction engineering of Shandong province.

## Nomenclature

$\Delta A_p$ – pore surface area, [m$^2$]
$a_{af}$ – specific surface area of porous materials, [m$^{-1}$]
$F_n(x)$ – eigenfunction
$h_e$ – interstitial heat transfer coefficient, [Wm$^{-2}$K$^{-1}$]
$k$ – thermal conductivity, [Wm$^{-1}$K$^{-1}$]
$L$ – porous material thickness, [m]
$Nn$ – norm
$q(x, t)$ – heat flux, [Wm$^{-2}$]
$r_h$ – hydraulic radius, $\Delta V_p/\Delta A_p$, [m]
$S$ – volumetric heat source, [Wm$^{-3}$]
$t_{min}$ – entry moment to the LTNE condition, [s]
$t_{max}$ – exit moment to the LTNE condition, [s]
$\Delta t$ – duration of the LTNE condition, [s]
$T(x, t)$ – temperature distribution, [K]
$T_0$ – initial temperature, [K]
$T_{st}^*$ – steady-state temperature, [K]
$\vec{U}$ – velocity vector of fluid, [ms$^{-1}$]
$\Delta V_p$ – volume of a mean pore, [m$^3$]
$x$ – space co-ordinate in x-direction, [m]

*Greek symbols*

$\varepsilon$ – porosity of porous material $\varepsilon = V_a/V$
$\theta$ – dimensionless temperature
$\gamma_n$ – eigenvalue
$\rho C$ – heat capacity/unit volume, [Jm$^{-3}$K$^{-1}$]
$\tau_t$ – lag time of the temperature gradient [s]
$\tau_q$ – lag time of the heat flux [s]
$\tau_e$ – $[= (1 - \varepsilon)(\rho C)_f \tau_t/\rho C]$

*Subscripts*

a – air phase
f – fiber phase
e – effective property

## Appendix

This appendix details the solution of the governing equations eqs. (1)-(3) under four different boundary conditions listed in tab. 1 and fig. 2. The temperature distribution of each model can be derived as follow based on the analytical approach [7]. In the present work, the boundary conditions are considered as the non-flow or negligible flow cases, therefore the natural convection can be ignored generally [31, 32] if there is no flow blow-in from the boundaries.

The air phase solution of **B.C.1** can be solved as:

$$T_a = \sum_{n=0}^{\infty} \frac{q_0 \cos\left[(2n+1)\dfrac{\pi x}{2L}\right]}{\rho CL(\tau_q + \tau_e)\omega_n} \left[\frac{-2\omega_n + (\omega_n + a_n)e^{(\omega_n - a_n)t}(\omega_n - a_n)e^{-(\omega_n + a_n)t}}{\omega_n^2 - a_n^2}\right] \quad \text{(A.1a)}$$

The fiber phase temperature distribution can be solved from the relation defined in eq. (2), in addition, the interstitial heat transfer $h_e$ can be replaced as $h_e = \mathrm{Nu}_{rh} k_a/r_h$, the Nusselt number $\mathrm{Nu}_{rh}$ is about 1 and $t_q$ is set as zero, in the no flow case of ref. [7], so:

$$T_f = T_a + \frac{r_h \rho C_a}{h_e}\frac{\partial T_a}{\partial t} = T_a + \frac{r_h^2 \rho C_a}{\mathrm{Nu}_{rh} k_a}\sum_{n=0}^{\infty}\frac{q_0 \cos\left[(2n+1)\dfrac{\pi x}{2L}\right](e^{(\omega_n - a_n)t}e^{-(\omega_n + a_n)t}}{\rho CL(\tau_q + \tau_e)\omega_n} \quad \text{(A.1b)}$$

We then obtain the dimensionless temperature distribution of each phase:

$$\theta_a = \frac{T_{st} - T_a}{T_{st}} \quad \theta_f = \frac{T_{st} - T_f}{T_{st}} \quad \text{(A.1c)}$$

where symbols

$$a_{\mathrm{n}} = \gamma_{\mathrm{n}} - \beta_{\mathrm{n}},\ \omega_{\mathrm{n}} \sqrt{\beta_n^2 - \lambda_n^2},\ \beta_{\mathrm{n}} = \gamma_{\mathrm{n}} \left[ 1 - \frac{1}{2} \frac{\tau_{\mathrm{t}}}{\tau_{\mathrm{q}} + \tau_{\mathrm{e}}} - \frac{1}{2\gamma_{\mathrm{n}} (\tau_{\mathrm{q}} + \tau_{\mathrm{e}})} \right],\ \lambda_{\mathrm{n}} = \gamma_{\mathrm{n}} \sqrt{1 - \frac{\tau_{\mathrm{t}}}{\tau_{\mathrm{q}} + \tau_{\mathrm{e}}}}$$

and

$$T_{\mathrm{st}} = \sum_{n=0}^{\infty} \frac{q_0 \cos\left[ (2n+1) \frac{\pi x}{2L} \right]}{\rho C L (\tau_{\mathrm{q}} + \tau_{\mathrm{e}}) \omega_{\mathrm{n}}} \frac{-2\omega_{\mathrm{n}}}{\omega_n^2 - a_n^2}$$

is the final steady-state temperature after non-linearly rise of the transient stage. The parameters ($F_{\mathrm{n}}(x)$, $N_{\mathrm{n}}$, and $\gamma_{\mathrm{n}}$) can be acquired and yielded in tab. A.1 under different boundary conditions.

**Table A.1. Calculated parameters for each boundary condition**

| | Eigenfunction $F_{\mathrm{n}}(x)$ ($n$ = 0, 1, 2, ...) | Eigenvalue $\gamma_{\mathrm{n}}$($n$ = 0, 1, 2, ...) | Norm *Nn* |
|---|---|---|---|
| B.C.1 | $F_{\mathrm{n}}(x) = \cos((2n + 1)\ \pi x/2L)$ | $\gamma_{\mathrm{n}} = [(2n + 1)\pi/2L]^2 k_{\mathrm{e}}/\rho C$ | $Nn = L/2$ |
| B.C.2 | $F_{\mathrm{n}}(x) = \cos(n\pi x/L)$ | $\gamma_{\mathrm{n}} = (n_{\mathrm{p}}/L)^2 k_{\mathrm{e}}/\rho C$ | $Nn = L$ $n = 0$ $Nn = L/2$ $n > 0$ |
| B.C.3 | $F_{\mathrm{n}}(x) = \sin(n\pi x/L)$ | $\gamma_{\mathrm{n}} = (n_{\mathrm{p}}/L)^2 k_{\mathrm{e}}/\rho C$ | $Nn = L/2$ |
| B.C.4 | $F_{\mathrm{n}}(x) = \cos((2n + 1)\pi x/2L)$ | $\gamma_{\mathrm{n}} = [(2n + 1)\pi/L)^2 k_{\mathrm{e}}/\rho C$ | $Nn = L/2$ |

Furthermore, the derivation of others three models (B.C.2~4) can be found as follow.

**B.C.2.**

The temperature distribution of air phase and fiber phase can be obtained:

$$T_a = \frac{q_0}{\rho C L} \left\{ \frac{-1 + (\omega_0 + a_0)t + \mathrm{e}^{-(\omega_0 + a_0)t}}{\omega_0 + a_0} + \right.$$

$$\left. + \sum_{n=1}^{\infty} \frac{q_0 \cos\left( \frac{n\pi x}{L} \right) \left[ -2\omega_{\mathrm{n}} + (\omega_{\mathrm{n}} + a_{\mathrm{n}}) \mathrm{e}^{(\omega_n - a_n)t} + (\omega_{\mathrm{n}} - a_{\mathrm{n}}) \mathrm{e}^{-(\omega_n + a_n)t} \right]}{(\tau_{\mathrm{q}} + \tau_{\mathrm{e}}) \omega_{\mathrm{n}} (\omega_n^2 - a_n^2)} \right\} \quad \text{(A.2a)}$$

$$T_{\mathrm{f}} = T_{\mathrm{a}} + \frac{r_h^2 \rho C_{\mathrm{a}}}{\mathrm{Nu}_{\mathrm{rh}} k_{\mathrm{a}}} \left\{ \frac{q_0}{\rho C L} (1 - \mathrm{e}^{-(\omega_0 + a_0)t} + \sum_{n=1}^{\infty} \frac{q_0 \cos\left( \frac{n\pi x}{L} \right)}{\rho C L} \left[ \frac{\mathrm{e}^{(\omega_n - a_n)t} - \mathrm{e}^{-(\omega_n + a_n)t}}{(\tau_{\mathrm{q}} + \tau_{\mathrm{e}}) \omega_{\mathrm{n}}} \right] \right\} \quad \text{(A.2b)}$$

The dimensionless temperature distribution:

$$\theta_{\mathrm{a}} = \frac{T_{\mathrm{ast}} - T_{\mathrm{a}}}{T_{\mathrm{ast}}}, \quad \theta_{\mathrm{f}} = \frac{T_{\mathrm{fst}} - T_{\mathrm{f}}}{T_{\mathrm{fst}}} \quad \text{(A.2c)}$$

where

$$T_{\mathrm{ast}} = \frac{q_0}{\rho C L} \left[ \frac{-1 + (\omega_0 + a_0)t}{\omega_0 + a_0} + \sum_{n=1}^{\infty} \frac{(-2\omega_{\mathrm{n}}) \cos\left( \frac{n\pi x}{L} \right)}{(\tau_{\mathrm{q}} + \tau_{\mathrm{e}}) \omega_n (\omega_n^2 - a_n^2)} \right] \text{ and}$$

$$T_{\mathrm{fst}} = \frac{q_0}{\rho C L}\left[\frac{r_h^2 \langle \rho C \rangle^a}{\mathrm{Nu}_{\mathrm{rh}} k_{\mathrm{a}}} + \frac{-1+(\omega_0 + a_0)t}{\omega_0 + a_0} + \sum_{n=1}^{\infty} \frac{(-2\omega_{\mathrm{n}})\cos\left(\dfrac{n\pi x}{L}\right)}{(\tau_{\mathrm{q}} + \tau_{\mathrm{e}})\omega_n(\omega_n^2 - a_n^2)}\right]$$ are the

linear temperatures arising during the quasi-steady stage of air and fiber phase, respectively.

**B.C.3**

$$T_{\mathrm{a}} = \frac{T_{\mathrm{h}}}{L}x + \sum_{n=1}^{\infty} \frac{2(-1)^n T_h \sin\left(\dfrac{n\pi x}{L}\right)}{n\pi}\left\{\frac{(a_{\mathrm{n}} + \omega_{\mathrm{n}})\,\mathrm{e}^{(\omega_n - a_n)t} - (\omega_n^2 - a_n^2)\,\mathrm{e}^{(\omega_n + a_n)t}}{2\omega_{\mathrm{n}}}\right\} \quad \text{(A.3a)}$$

$$T_{\mathrm{f}} = T_{\mathrm{a}} + \frac{r_h^2 \rho C_{\mathrm{a}}}{\mathrm{Nu}_{\mathrm{rh}} k_{\mathrm{a}}}\left\{\sum_{n=1}^{\infty} \frac{2(-1)^n T_h \sin\left(\dfrac{n\pi x}{L}\right)}{n\pi}\left[\frac{(\omega_n^2 - a_n^2)\,\mathrm{e}^{(\omega_n - a_n)t} - (\omega_n^2 - a_n^2)\,\mathrm{e}^{-(\omega_n + a_n)t}}{2\omega_{\mathrm{n}}}\right]\right\} \quad \text{(A.3b)}$$

The final temperature value of this model is $T_{\mathrm{f}}(x) = T_{\mathrm{a}}(x) = T_{\mathrm{h}}x/L$, so the dimensionless temperature distribution:

$$\theta_{\mathrm{a}} = \frac{T_{\mathrm{h}}x - T_{\mathrm{a}}L}{T_{\mathrm{h}}x}, \quad \theta_{\mathrm{f}} = \frac{T_{\mathrm{h}}x - T_{\mathrm{f}}L}{T_{\mathrm{h}}x} \quad \text{(A.3c)}$$

**B.C.4**

$$T_{\mathrm{a}} = T_{\mathrm{h}} - \sum_{n=1}^{\infty} \frac{2(-1)^n T_h \cos\left[(2n+1)\dfrac{\pi x}{2L}\right]}{(2n+1)\pi}\left\{\frac{(a_{\mathrm{n}} + \omega_{\mathrm{n}})\,\mathrm{e}^{(\omega_n - a_n)t} + (\omega_{\mathrm{n}} - a_{\mathrm{n}})\,\mathrm{e}^{-(\omega_n + a_n)t}}{\omega_{\mathrm{n}}}\right\} \quad \text{(A.4a)}$$

$$T_{\mathrm{f}} = T_{\mathrm{a}} - \frac{r_h^2 \rho C_{\mathrm{a}}}{\mathrm{Nu}_{\mathrm{rh}} k_{\mathrm{a}}}\left\{\sum_{n=1}^{\infty} \frac{2(-1)^n T_h \cos\left[(2n+1)\dfrac{\pi x}{2L}\right]}{(2n+1)\pi}\left[\frac{(\omega_n^2 - a_n^2)\,\mathrm{e}^{(\omega_n - a_n)t} - (\omega_n^2 - a_n^2)\,\mathrm{e}^{-(\omega_n + a_n)t}}{\omega_{\mathrm{n}}}\right]\right\} \quad \text{(A.4b)}$$

The dimensionless temperature distribution:

$$\theta_{\mathrm{a}} = \frac{T_{\mathrm{h}} - T_{\mathrm{a}}}{T_{\mathrm{h}}}, \quad \theta_{\mathrm{f}} = \frac{T_{\mathrm{h}} - T_{\mathrm{f}}}{T_{\mathrm{h}}} \quad \text{(A.4c)}$$

## References

[1] Cattaneo, C., About Heat Conduction (in Italian), Atti del Semin, Mat.e Fis. Univ. Modena, *3* (1948), pp. 83-101
[2] Vernotte, P., Paradoxes in the Continuous Theory of the Heat Equation, *C. R. Acad. Bulg. Sci., 246* (1958), pp. 3154-3155
[3] Tzou, D. Y., A Unified Field Approach for Heat Conduction From Macro- to Micro-Scales, *Journal of Heat Transfer, 117* (1995), 1, pp. 8-16
[4] Amiri, A., Vafai, K., Analysis of Dispersion Effects and Non-Thermal Equilibrium, Non-Darcian, Variable Porosity Incompressible Flow through Porous Media, *International Journal of Heat and Mass Transfer, 37* (1994), 6, pp. 939-954
[5] Nield, D.A., *et al.*, Effect of Local Thermal Non-Equilibrium on Thermally Developing Forced Convection in a Porous Medium, *International Journal of Heat and Mass Transfer, 45* (2002), 25, pp. 4949-4955
[6] Kuznetsov, A. V., An Investigation of a Wave of Temperature Difference between Solid and Fluid Phases in a Porous Packed Bed, *International Journal of Heat and Mass Transfer, 37* (1994), 18, pp. 3030-3033

[7] Minkowycz, W. J., *et al*., On Departure from Local Thermal Equilibrium in Porous Media Due to a Rapidly Changing Heat Source: the Sparrow Number, *International Journal of Heat and Mass Transfer, 42* (1999), 18, pp. 3373-3385
[8] Lee, D.Y., Vafai, K., Analytical Characterization and Conceptual Assessment of Solid and Fluid Temperature Differentials in Porous Media, *International Journal of Heat and Mass Transfer, 42* (1999), 3, pp. 423-435
[9] Yang, K., *et al*., Analysis of Temperature Gradient Bifurcation in Porous Media – An Exact Solution, *International Journal of Heat and Mass Transfer, 53* (2010), 19-20, pp. 4316-4325
[10] Vadasz, P., On the Paradox of Heat Conduction in Porous Media Subject to Lack of Local Thermal Equilibrium, *International Journal of Heat and Mass Transfer, 50* (2007), 21-22, pp. 4131-4140
[11] Zhao, L., *et al*., Fractal Approach to Flow through Porous Material, *International Journal of Nonlinear Sciences and Numerical Simulation, 10* (2009), 7, pp. 857-902
[12] Shi, X.-J., Yu, W. D., Fractal Phenomenon in Micro-Flow through a Fiber Bundle, *International Journal of Nonlinear Sciences and Numerical Simulation, 10* (2009), 7, pp. 861-866
[13] Li, Z.-B., He, J.-H., Fractional Complex Transform For Fractional Differential Equations, *Mathematical and Computational Application, 15* (2010), 5, pp. 970-973
[14] Li, Z.-B., An Extended Fractional Complex Transform, *International Journal of Nonlinear Sciences and Numerical Simulation, 11* (2010), Suppl., pp. 135-337
[15] He, J.-H., A New Fractal Derivation, *Thermal Science, 15* (2011), Suppl. 1, pp. S145-S147
[16] Fan, J., *et al.*, Hierarchy of Wool Fibers and Fractal Dimensions, *International Journal of Nonlinear Sciences and Numerical Simulation, 9* (2008), 3, pp. 293-296
[17] Yang, X.-J., *et al.*, Fractal Heat Conduction Problem Solved by Local Fractional Variation Iteration Method, *Thermal Science, 17* (2012), 3, pp. 707-713
[18] Lee, J., *et al.*, Effect of Thermal Non-Equilibrium on Convective Instability in a Ferromagnetic Fluid-Saturated Porous Medium, *Transport In Porous Media, 86* (2011), 1, pp. 103-124
[19] Nouri-Borujerdi, A., *et al*., The Effect of Local Thermal Non-Equilibrium on Conduction in Porous Channels with a Uniform Heat Source, *Transport in Porous Media, 69* (2007), 2, pp. 281-288
[20] Hayes, A. M., *et al.*, The Thermal Modeling of a Matrix Heat Exchanger Using a Porous Medium and the Thermal Non-Equilibrium Model, *International Journal of Thermal Sciences, 47* (2008), 10, pp. 1306-1315
[21] Tian, M., *et al*., Measuring the Thermophysical Properties of Porous Fibrous Materials with a New Unsteady-State Method, *Journal of Thermal Analysis and Calorimetry, 107* (2012), 1, pp. 395-405
[22] Xu, F., *et al*., Modeling Skin Thermal Pain Sensation: Role of Non-Fourier Thermal Behavior in transduction Process of Nociceptor, *Computers in Biology and Medicine, 40* (2010), 5, pp. 478-486
[23] Tian, M., *et al.*, Skin Thermal Stimulation on Touching Cool Fabric from the Transient Stage to Steady-State Stage, *International Journal of Thermal Sciences, 53* (2012), March, pp. 80-88
[24] Pan, N., *et al.*, Fibrous Materials as Soft Matter, *Textile Res. J., 77* (2007), 4, pp. 205-213
[25] Wang, X. Y., *et al*., Abrasion Resistance of Thermally Bonded 3D Nonwoven Fabrics, *Wear, 262* (2007), 3-4, pp. 424-431
[26] Amiri, A., *et al*., Transient Analysis of Incompressible Flow through a Packed Bed, *International Journal of Heat and Mass Transfer, 41* (1998), 24, pp. 4259-4279
[27] Wang, L., *et al*., Equivalence between Dual-Phase-Lagging and Two-Phase-System Heat Conduction Processes, *International Journal of Heat and Mass Transfer, 51* (2008), 7-8, pp. 1751-1756
[28] Kim, K. J., *et al*., Thermal Conduction between a Heated Microcantilever and a Surrounding Air Environment, *Applied Thermal Engineering, 29* (2009), 8-9, pp. 1631-1641
[29] Tian, M., *et al*., Effects of Layer Stacking Sequence on Temperature Response of Multi-Layer Composite Materials under Dynamic Conditions, *Applied Thermal Engineering, 33-34* (2012), Feb., pp. 219-226
[30] Hammerschmidt, U., A Quasi-Steady State Technique to Measure the Thermal Conductivity, *International Journal of Thermophysics, 24* (2003), 5, pp. 1291-1312
[31] Farnworth, B., Mechanisms of Heat Flow through Clothing Insulation *Textile Research Journal, 53* (1983), 12, pp. 717-725
[32] Tian, M., *et al*., Effects of Layering Sequence on Thermal Response of Multilayer Fibrous Materials: Unsteady-State Cases, *Experimental Thermal and Fluid Science, 41* (2012), Apr., pp. 143-148

Paper submitted: June 7, 2012
Paper revised: January 7, 2013
Paper accepted: March 5, 2013